Outlets Airflow Velocity Enhancement of an Automotive HVAC Duct

N. Olleh
School of Mechanical Engineering, Faculty of Engineering, Universiti Teknologi Malaysia

N.A. Husain
School of Mechanical Engineering, Faculty of Engineering, Universiti Teknologi Malaysia

H.M. Kamar
School of Mechanical Engineering, Faculty of Engineering, Universiti Teknologi Malaysia

N.B. Kamsah
School of Mechanical Engineering, Faculty of Engineering, Universiti Teknologi Malaysia

他

https://doi.org/10.5109/4372273

出版情報：Evergreen. 8 (1), pp.163-169, 2021-03. 九州大学グリーンテクノロジー研究教育センター
バージョン：

Outlets Airflow Velocity Enhancement of an Automotive HVAC Duct

N. Olleh[1], N.A. Husain[1], H.M. Kamar[1,*], N.B. Kamsah[1], M. Idrus Alhamid[2]

[1]School of Mechanical Engineering, Faculty of Engineering, Universiti Teknologi Malaysia, 81310 UTM Johor Bahru, Johor, Malaysia

[2]Departemen Teknik Mesin, Fakultas Teknik, Universitas Indonesia, Kampus Baru – UI, Depok 16424, Indonesia

*Corresponding Author's email: haslinda@utm.my

(Received November 27, 2020; Revised January 30, 2021; accepted March 23, 2021).

Abstract: Heating, ventilation, air-conditioning (HVAC) duct system for an automotive has a complex geometry due to space constraints in the engine compartment. This could reduce air pressure inside the duct, decreasing the airflow velocity at the HVAC outlets, and correspond to the intended value prescribed by design. Higher air velocity at the ventilation outlets is desirable to promote thermal comfort in the passenger cabin. This study aims to enhance the airflow velocity and uniformity at each duct outlet by varying outlet geometry and duct elbow angles using the computational fluid dynamics (CFD) method. A typical HVAC duct of a C-segment car has been chosen as the case study. Steady-state parametric flow analyses were conducted to determine the duct geometry that would significantly improve the airflow uniformity and velocity at the duct outlets. It was found that a combination of circular outlets with a 65° elbow angle results in the best improvement in the airflow velocity distribution inside the duct. It was also found that the airflow velocity at the outlets increases between 4% to 9% compared to the baseline design. The air velocity difference between all outlets is around 1.3%, which can be considered negligibly small.

Keywords: Automotive HVAC duct; airflow velocity; computational fluid dynamics

1. Introduction and background

Passengers' thermal comfort inside a car cabin can be obtained by employing a heating, ventilation, and air-conditioning (HVAC) system on the vehicle. However, the ideal level of thermal comfort could not be achieved if the magnitude of the airflow velocity at the ventilation outlets was not obtained as intended by design, at any given climatic conditions [1) 2) 3) 4) 5)]. This problem is due to reduced airflow pressure at a specific point within the duct, caused by several factors such as HVAC duct size, duct geometry, air vents geometry, and outlet vents arrangement. According to ASHRAE (2011)[6)], an HVAC duct should have an excellent performance when it could provide sufficient airflow velocity to all the ventilation outlets and produce insignificant pressure drop. At the same time, it does not produce rush noise. Fabio et al. (2015)[7)] have also established that pressure losses and airflow characteristics are the criteria to predict duct performance. Uniformity of the airflow at the ventilation outlets is another criterion to measure the HVAC duct[8)].

The flow field profile in an HVAC duct has a significant impact on the temperature distribution and passenger thermal comfort inside the vehicle cabin[9)]. The effective operation of ventilation outlets depends on apparent details in the HVAC duct design and the flow history in the supply channel[10)]. As an engine compartment has limited space to house the HVAC duct as intended by design, it must be based on the designated area. Many studies were conducted to examine the effects of various duct and vent outlets' design on the airflow velocity. The methods used are diverse. Experimental investigations involve airflow visualization approach through a smoke test and airflow velocity measurement using a hot-wire anemometer. In contrast, the numerical approach, the majority of the studies used the computational fluid dynamics (CFD) technique for visualizing the airflow profile along the duct [2) 3) 4) 9) 10) 11) 12) 13) 14)].

Spalart-Allmaras is a model used for a modified eddy viscosity, and it is not suitable for 3D flows, free shear flows, and flows with strong separation[15)]. The *k-ε* turbulence model offers more vigorous and reasonably accurate results[16)]. It also feeds the elements of compressibility, buoyancy, and combustion features. However, it performs poorly for strong separation, large streamline curvature, and significant pressure gradient[17)].

The RNG *k-ε* was designed to overcome the latter problems[18]. It gives better performance compared to the Standard *k-ε* for more complex shear flow. Besides, it is also suitable for flows with high strain rates, swirls, and separation. The *k-ω* turbulence model gained popularity due to its accurateness and robustness for a wide range of boundary layer flows with a pressure gradient. It provides several options to solve compressibility effects, transitional flows, and shear-flow corrections. It is also more sensitive to the free-stream condition and improved its behavior under an adverse pressure gradient[19]. Another frequent turbulence model used in the CFD analysis is SST *k-ω*, categorized under the k-ω turbulence family. The SST *k-ω* model uses a blending function to gradually transition from the standard *k-ω* model near the wall to a high-Reynolds-number version of the *k–ε* model in the outer portion of the boundary layer. Transport effects of the principal turbulent shear stress were accounted for by using modified turbulent viscosity formulation [3) 19) 20) 21) 22) 23) 24) 25)].

This study aims to enhance the airflow velocity and uniformity at each duct outlet by varying outlet geometry and duct elbow angles using the CFD method. This method is capable of performing a rigorous analysis and more economical when compared to experimental works. Furthermore, it could evaluate the performance of a full range of system configurations on the computer without the time, expense, and disruption required to make actual changes onsite. The technique uses numerical schemes to solve the fundamental nonlinear differential equations that describe fluid flow (the Navier-Stokes and allied equations) for predefined geometries and boundary conditions.

2. CFD analysis implementation

A computational fluid dynamic (CFD) method was employed to carry out a steady-state flow analysis on the HVAC duct. This involves constructing simplified geometries of the computational domain, meshing the domain, prescribing the boundary conditions, choosing a suitable airflow model, setting the solution method, and specifying convergence tolerances. A parametric study was carried out to examine the effects of modifying the duct geometry on airflow velocity and pressure distributions inside the duct.

2.1 Geometry of the computational domain

A simplified 3D model of the HVAC duct was developed using CAD software. It is shown in Fig. 1. The geometry used is based on the actual duct for a Proton Persona passenger car. It has one inlet and four outlets. The present geometry is considered as the baseline model.

The duct has a width of 1278 mm and a height of 387 mm. The inlet is square with a length of 276 mm and a width of 86 mm. Dimensions of outlets 1 (same as outlet 4) and 2 (same as outlet 3) are shown in Fig. 2.

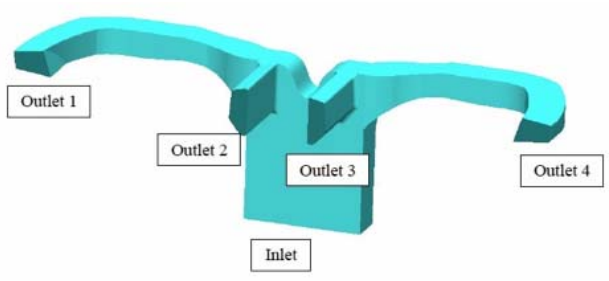

Fig. 1: Geometry of the computational domain

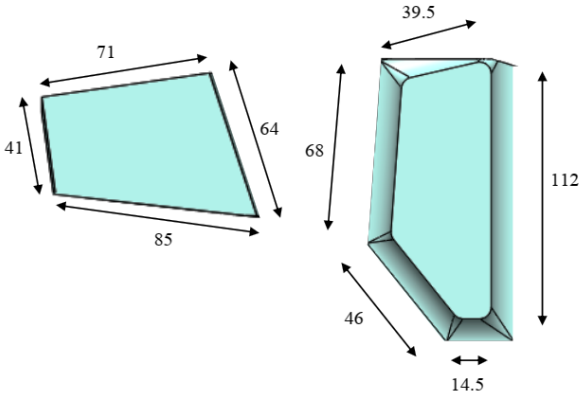

Fig. 2: Dimension of outlet ducts 1 and 2 (in mm)

2.2 Meshing of the computational domain

The geometry meshed with unstructured tetrahedral elements. This element type was chosen because it is suitable to be used in complex geometry. Tetrahedral elements are also entirely accurate and stable for steady-state flow analysis. The meshed geometry is shown in Fig. 3.

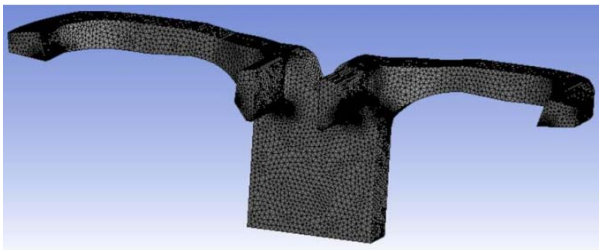

Fig. 3: Meshed computational domain

The minimum and maximum element sizes were set as 0.8 and 11 mm, respectively. This setting produces 639,460 elements for the domain. These numbers were obtained from a grid-independent test (GIT) performed on the CFD model. With this number of elements, the mesh quality was found to be 0.8337, and the skewness was 0.2327, indicating an excellent overall mesh quality.

2.3 Boundary conditions for baseline model

An inflow mass flux of 0.16 kg/s was specified at the inlet of the baseline model. This is based on the car manufacturer's data, which was based on the maximum blower speed condition at the inlet. A wall boundary

condition was enforced on all faces bounding the flow domain. The wall surfaces were prescribed as a no-slip condition. A zero-gage pressure condition was prescribed at all four outlets of the duct. The boundary conditions are illustrated in Fig. 4.

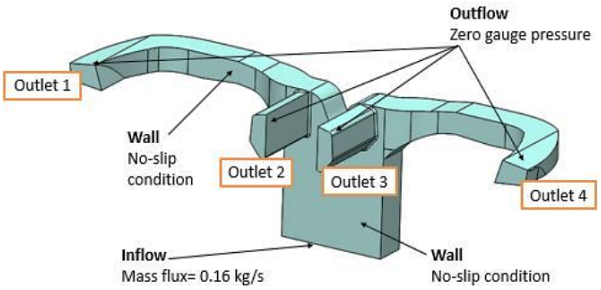

Fig. 4: The prescribed boundary condition

2.4 Analysis setup for baseline model

A pressure-based solver is used as the solution method. This solver is applicable for a wide range of flow regimes from low-speed incompressible flow to high-speed compressible flow. It requires less storage memory and allows flexibility in the solution procedure. Residual history is used to monitor the convergence of the solution. The number of iterations was set at 1000 to ensure a sufficient convergence of the solution. A Standard k-ε was used as an initial turbulence model. The most suitable turbulence model will be determined through a model validation process. Also, an enhanced wall function was applied.

2.5 Grid-independent test

A grid-independent test (GIT) was carried on the baseline model to determine the adequate number of elements that would produce the smallest error in the simulation results. This test was first done by carrying out a steady-state flow simulation using a relatively coarse meshing. The number of elements was then gradually increased, and the flow simulation was repeated for each element increment. Five cases were considered in the test. In the first case, the maximum element size was set at 11 mm. Then, the element size was repeatedly reduced by 1 mm for the remaining cases. For each case, the average airflow velocity at all outlets was observed. Figure 5 shows a plot of the average airflow velocity at all outlets for all cases.

Let us consider the results for case 3 and case 4. It can be seen that the difference in the airflow velocity at all outlets is the smallest, i.e., less than 3%, between these two cases. Thus, the number of elements for case 3, which is 693,460, was chosen for the CFD model. It would produce reasonably good results and requires shorter computational time to complete the flow simulation compared to case 4. Case 5 involves a much larger number of elements and thus requires a much longer computational time to complete the simulation. Therefore, it was not considered in this study.

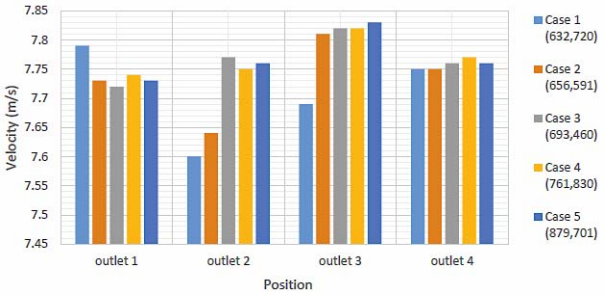

Fig. 5: Airflow velocity at duct outlets for all cases

2.6 Validation of flow model

This process was carried out to identify the most suitable turbulent flow model used in the flow simulations. Five flow models were considered in this study: the k-ε Standard, k-ε Realizable, k-ε RNG, k-ω Standard, and k-ω SST. These are two-equation models that are usually used for internal flow analysis, especially in ducting applications. Steady-state flow simulations were carried out, employing each flow model. For each flow model, the average airflow velocity at all duct outlets was observed and compared with the manufacturer's experimental data.

Table 1: Errors in airflow velocity at duct outlets

Position	Turbulence Model				
	k-ε Standard	k-ε Reliazable	k-ε RNG	k-ω Standard	k-ω SST
Outlet 1	7.43	7.67	6.59	6.59	6.59
Outlet 2	6.39	5.78	5.54	3.37	2.53
Outlet 3	9.07	8.14	8.37	8.26	7.33
Outlet 4	9.24	9.24	8.42	8.30	8.19

The percent errors in the average airflow velocity at each duct outlet compared to the experimental values are tabulated in Table 1 for all the flow models considered in this study. It can be observed that the errors associated with the k-ω SST flow model are the smallest, i.e., ranging from 2% to 8%, compared to the other flow models. Based on this finding, the k-ω SST turbulent flow model was chosen for the proceeding flow simulations on the CFD model.

2.7 Parametric analysis

A parametric analysis was carried out in this study to examine the effects of outlet shape and elbow angle of the duct on the airflow velocity at all the outlets. Five cases of duct modification were considered. These cases are summarized in Table 2 and illustrated in Fig. 6. Case 1 refers to the baseline case.

Table 2: Duct modifications for a parametric analysis

Case	Factor
1	Baseline outlet shape
2	Circular shape for outlet 1 and 4
3	Circular shape for outlet 2 and 3
4	Circular shape for outlet 1, 2, 3, and 4
5	Circular outlet with 70° elbow angle
6	Circular outlet with 65° elbow angle

A circular-shape outlet offers the least resistance in delivering out air from the duct. An equivalent-area concept was used in transforming the present outlet shapes into the circular shape. In case 2, the equivalent diameter of outlets 1 and 4 is 35.2 mm, while in case 3, the equivalent diameter of outlets 2 and 3 is 35.4 mm.

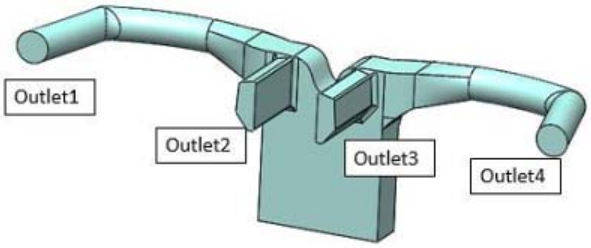

(a) Case 2

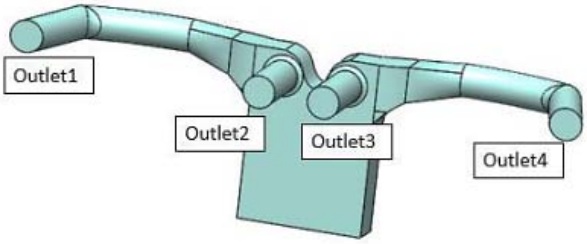

(b) Case 3

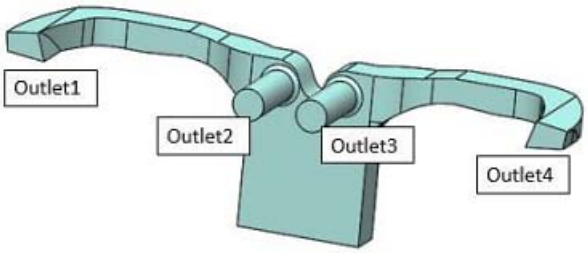

(c) Case 4

Fig. 6: Modifications on the duct outlets shape

An appropriate elbow angle will ensure the smoothness of the airflow through the HVAC duct. Smooth airflow will increase the airflow velocity at the outlets. In this parametric study, the elbow angle corresponding to outlet 1 and outlet 4 was modified from the current value of 75°. In case 5, the elbow was reduced to 70°, while in case 6, the angle was reduced further to 65°. All the elbow angle modifications were based on case 4, where all outlets' shape is circular. These are illustrated in Fig. 7.

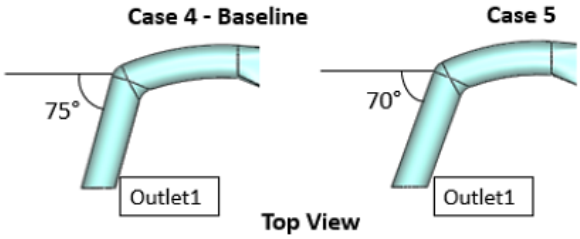

(a) Case 5

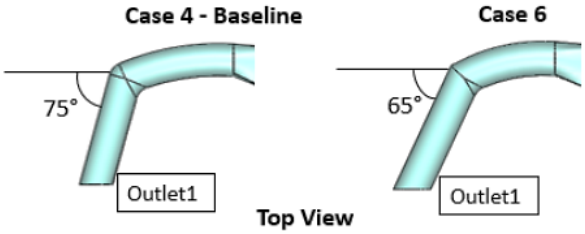

(b) Case 6

Fig. 7: Modification on the elbow angle corresponding to outlet 1 and outlet 4 (not shown)

3. Results and discussion

3.1 Airflow velocity distribution: baseline case

Figure 8 shows the airflow velocity distribution inside the HVAC duct for the baseline case.

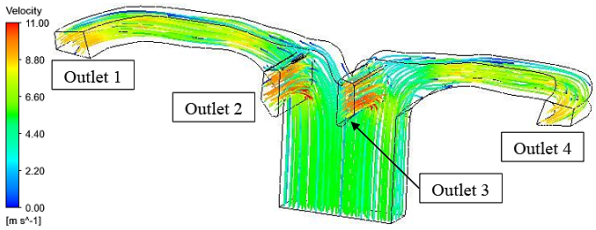

Fig. 8: Airflow velocity distribution for the baseline case

It can be seen from the figure that the airflow velocity is nearly uniform at the inlet and through the vertical section of the HVAC duct, with a magnitude of about 5 m/s. The airflow velocity increases in magnitude along with the horizontal elbows, i.e., around 7 m/s since there is less resistance to the flow. The airflow velocity magnitude gets even higher at the duct's outlets as the air leaves the duct to a lower atmospheric pressure region. It was found that the airflow velocity magnitude at outlets 1, 2, 3, and 4 are 7.8 m/s, 8 m/s, 8 m/s, and 7.9 m/s, respectively. This indicates that the airflow is nearly equally distributed to all the duct outlets, which is desirable.

The distribution of airflow distribution inside the duct for case 2 is shown in Fig. 9. It can be observed that the airflow velocity distribution inside the vertical section of the duct remains nearly uniform with a magnitude almost similar to the baseline case. However, the magnitude of the airflow velocity inside the horizontal sections and at all the outlets is higher than the baseline case. It was found that the airflow velocity magnitude at outlets 1, 2, 3, and 4 are 8.2 m/s, 8 m/s, 8 m/s, and 8.2 m/s, respectively. This indicates that the airflow is equally distributed to all the duct outlets. The percent increase in the airflow velocity magnitude at outlets 1, 2, 3, and 4 is around 5%, 0%, 1%, and 4%, respectively. This finding shows that the airflow velocity magnitude increases at nearly similar percent at outlets 1 and 4, modified into a circular shape.

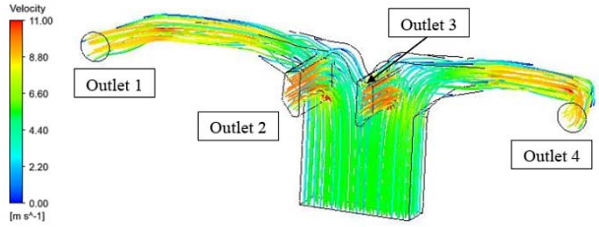

Fig. 9: Airflow velocity distribution for case 2

Figure 10 shows the airflow velocity distribution for case 3, where the geometry of outlets 2 and 3 was modified into a circular shape. It can be observed that the airflow velocity distribution inside the vertical and horizontal sections of the duct exhibits a similar pattern as those for the baseline case. However, the airflow velocity at outlets 2 and 3 is higher in magnitude.

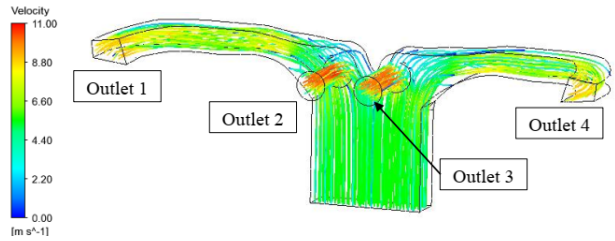

Fig. 10: Airflow velocity distribution for case 3

The magnitude of airflow velocity at outlets 1, 2, 3, and 4 is 8 m/s, 8.6 m/s, 8.5 m/s, and 8 m/s, respectively, which again indicates that the airflow is distributed equally to all the duct exit. Compared to the baseline case, the percent increase in the airflow velocity at outlet 1, 2, 3, and 4 is about 2%, 6%, 7%, and 1%, respectively.

The airflow velocity distribution for case 4, in which all outlets' geometry was modified into a circular shape, is shown in Fig. 11. It can be seen that with the outlet's modification, the airflow velocity inside the horizontal

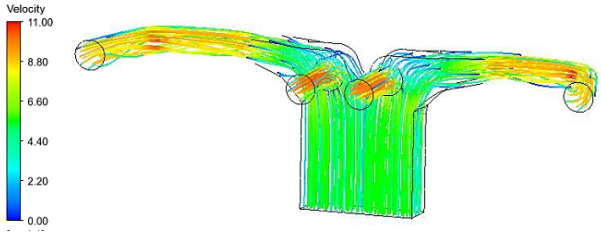

Fig. 11: Airflow velocity distribution for case 4

sections of the duct increase dramatically, i.e., in the range of 8 to 10 m/s in magnitude. The airflow velocity at outlets 1, 2, 3, and 4 was 8.4 m/s, 8.6 m/s, 8.6 m/s, and 8.4 m/s, respectively, indicating that the airflow is equally distributed to all the duct outlets. Compared to the baseline case, the percent increase in the airflow velocity at outlets 1, 2, 3, and 4 is 8%, 6%, 8%, and 7%, respectively. This case can be considered the best, which involves changing its geometry from the original shape to a circular one.

The distribution of airflow velocity inside the duct when its elbow angle was modified from the original value of 75° to 70° is shown in Fig. 12. This modification was based on the duct of case 4, in which all outlets have a circular shape. With this modification, the airflow velocity at outlets 1, 2, 3, and 4 was 8.5 m/s, 8.4 m/s, 8.6 m/s, and 8.5 m/s, respectively. Compared to case 4, it is clear that the reduction of the elbow angle from 75° to 70° does not result in an appreciable increase in the airflow velocity at all the duct outlets.

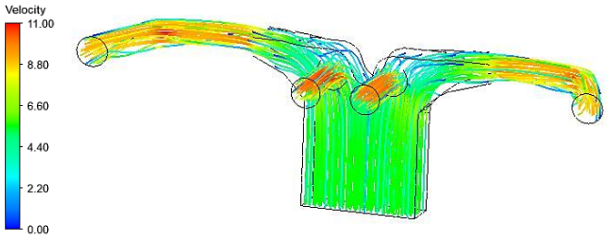

Fig. 12: Airflow velocity distribution for case 5

Figure 13 shows the airflow velocity distribution for the last case, i.e., case 6, in which the elbow angle for the duct of case 4 was modified further to 65°. It was found that the airflow velocity at outlets 1, 2, 3, and 4 is 8.5 m/s, 8.4 m/s, 8.6 m/s, and 8.5 m/s, respectively. When compared to the corresponding values for case 4, it is seen that the elbow angle modification does not produce any insignificant changes in the airflow velocity magnitude at all the duct outlets.

A steady-state airflow analysis through a simplified model of an HVAC duct for a Proton passenger car was carried out using a computational fluid dynamic (CFD) method. The duct's CFD model was validated based on the experimental data of airflow velocity at the outlets.

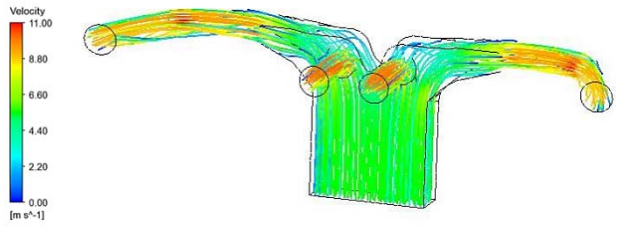

Fig. 13: Airflow velocity distribution for case 6

It was found that for the baseline case, corresponding to the original duct geometry and outlets shape, the airflow velocity distribution at the inlet and vertical section of the duct is nearly uniform at around 5 m/s. The airflow velocity magnitude increases as the airflow through the horizontal sections, i.e., around 7 m/s, and becomes slightly higher, i.e., around 8 m/s, at the outlets. Modifications were made on the shape of the outlets and the elbow angle of the original duct. It was found that when the shape of all outlets was changed to a circular shape, the airflow velocity magnitude at the outlets increases by around 6% to 8%, compared to the baseline case. Changing the elbow angle of the modified duct, i.e., when all the outlets have a circular shape, does not produce appreciable changes in the magnitude of the airflow velocity at all the outlets.

4. Conclusions

A steady-state airflow analysis through a simplified model of an HVAC duct for a Proton passenger car was carried out using a computational fluid dynamic (CFD) method. The duct's CFD model was validated based on the experimental data of airflow velocity at the outlets. It was found that for the baseline case, corresponding to the original duct geometry and outlets shape, the airflow velocity distribution at the inlet and vertical section of the duct is nearly uniform at around 5 m/s. The airflow velocity magnitude increases as the airflow through the horizontal sections, i.e., around 7 m/s, and becomes slightly higher, i.e., around 8 m/s, at the outlets. Modifications were made on the shape of the outlets and the elbow angle of the original duct. It was found that when the shape of all outlets was changed to a circular shape, the airflow velocity magnitude at the outlets increases by around 6% to 8%, compared to the baseline case. Changing the elbow angle of the modified duct, i.e., when all the outlets have a circular shape, does not produce appreciable changes in the magnitude of the airflow velocity at all the outlets.

Acknowledgements

The authors are grateful to the Universiti Teknologi Malaysia for providing funding for this study, with vote number 00L45. The financial support is managed by the Research Management Centre (RMC) Universiti Teknologi Malaysia.

References

1) A. G. Alam, A. Tirta and C. K. Priambada, "Building Beneficial Roof Insulation in Vertical Housing: Physical and Economical Selection Method," *Evergreen,* vol. 6, no. 2, pp. 124-133, (2019).
2) H. Han, M. Hatta and H. Rahman, "Smart Ventilation for Energy Conservation in Buildings," *Evergreen*, vol. 6, no. 6, pp. 44-51, (2019).
3) H. M. Kamar, N. Kamsah, F. N. Ghalib and M. I. Alhamid, "Enhancement of thermal comfort in a large space building," *Alexandria Engineering Journal*, vol. 58, no. 1, pp. 49-65, (2019).
4) D. W. Lee, "Impact of a three-dimensional air-conditioning system on thermal comfort: An experimental study," *International Journal of Automotive Technology*, vol. 16, no. 3, pp. 411-416, (2015).
5) Ali, S.M. and Chakraborty, A., "Performance Study of Adsorption Cooling Cycle for Automotive Air-conditioning," *Evergreen*, vol. 2, no. 1, pp. 12-22, (2015).
6) ASHRAE, Applications (SI), *ASHRAE* Inc., Atlanta, USA, (2011).
7) F. Fabio, O. Daniele and P. Stamatina, "Multiobjective Duct Optimization with Open Source CFD Solver," in *6th BETA CAE International Conference*, THESSALONIKI, GREECE, (2015).
8) B. Vasanth, M. Khan, N. Garikipati, S. Narayana and M. Govindarajalu, "Optimization of Center Console Duct using Robust Assessment Methodology," *SAE Technical Paper*, Vols. No. 2018-01-0072, (2018).
9) K. Rajdev, K. S. Jaswal and K. Vibhay, "Fluid flow analysis of HVAC Duct in Tractor cabin," in *Altair Technology Conference*, Chennai, India, (2017).
10) Lizal, O. Pech, J. Jedelsky, J. Tuhovcak and M. Jicha, "The automotive ventilation test case: Investigation of the velocity field downstream of a benchmark vent using smoke visualization and hot-wire anemometry," in *Proceedings of the Institution of Mechanical Engineers*, Part D: Journal of Automobile Engineering, (2018).
11) A. Tzanakis, "*Duct optimization using CFD software' ANSYS Fluent Adjoint Solver*," Goteborg, (2014).
12) C. Manu and K. Gunjan, "Numerical Simulation and Flow Analysis of Rear Transfer Ducts Using AcuSolve," in *India Altair Technology Conference*, Chennai, India, (2017).
13) Halawa, Amr M., Basman Elhadidi, and Shigeo Yoshida. "Aerodynamic performance enhancement using active flow control on DU96-W-180 wind turbine airfoil," *Evergreen*, vol. 5, no. 1, pp. 16-24, (2018).
14) Yinn, W. K., Kamar, H. M., Kamsah, N., & Norazam, A. S. "Effects of surgical staff turning

motion on airflow distribution inside a hospital operating room," *Evergreen*, vol. 6, no. 1, pp. 52-58, (2019).
15) S. R. Allmaras and F. T. Johnson, "Modifications and clarifications for the implementation of the Spalart-Allmaras turbulence model," in *In Seventh International Conference on Computational Fluid Dynamics (ICCFD7)*, (2012).
16) K. Stapleton, E. Guentsch, M. Hoskinson and W. Finlay, "On the suitability of k–ε turbulence modeling for aerosol deposition in the mouth and throat: a comparison with experiment," *Journal of Aerosol Science*, vol. 31, no. 6, pp. 739-749, (2000).
17) Fluent ANSYS, "http://www.southampton.ac.uk," 2006. [Online]. Available: *http://www.southampton.ac.uk/~nwb/lectures/GoodPracticeCFD/Articles/Turbulence_Notes_Fluent-v6.3.06.pdf*. [Accessed 05 October 2018].
18) J.-J. Kim and J.-J. Baik, "A numerical study of the effects of ambient wind direction on flow and dispersion in urban street canyons using the RNG k–ε turbulence model," *Atmospheric Environment*, vol. 38, no. 19, pp. 3039-3048, (2004).
19) W. Chan, P. Jacobs and D. Mee, "Suitability of the k–ω turbulence model for scramjet flow field simulations," *International Journal for Numerical Methods in Fluids*, vol. 70, no. 4, pp. 493-514, (2012).
20) H. M. Kamar, N. Kamsah and A. M. Mohammad Nor, "Numerical analysis of air-flow and temperature field in a passenger car compartment," in *AIP Conference Proceedings*, (2012).
21) C. John, D. O'Connor, P. Sofotasiou and B. Hughes, "CFD simulation and optimization of a low energy ventilation and cooling system," *Computation*, vol. 3, no. 2, pp. 128-149, (2015).
22) N. E. A. Shafie, H. M. Kamar and N. Kamsah, "Effects of air supply diffusers and air return grilles layout on contaminants concentration in bus passenger compartment," *International Journal of Automotive Technology*, vol. 17, no. 5, pp. 751-762, (2016).
23) L. Zhang, T. T. Chow, C. F. Tsang, K. F. Fong and L. S. Chan, "CFD study on effect of the air supply location on the performance of the displacement ventilation system," *Building and Environment*, vol. 40, no. 8, pp. 1051-1067, (2005).
24) Takeyeldein, M.M., Lazim, T.M., Ishak, I.S., Nik Mohd, N.A.R. and E.A., Ali, "Wind Lens Performance Investigation at Low Wind Speed," *Evergreen*, vol. 7, issue 4, pp. 00-00, (2020).
25) Ibrahim O.M, S., Yoshida, "Experimental and Numerical Studies of a Horizontal Axis Wind Turbine Performance over a Steep 2D Hill," *Evergreen*, vol. 5, no. 3, pp. 12-21, (2018).